FEATURE ARTICLE

Single Molecule Raman Spectroscopy at the Junctions of Large Ag Nanocrystals

Jiang Jiang, Ken Bosnick, Mathieu Maillard, and Louis Brus*

Chemistry Department, Columbia University, New York, New York 10027

Received: March 12, 2003; In Final Form: June 26, 2003

Molecular surface enhanced Raman scattering (SERS) in compact clusters of 30−70 nm Ag nanocrystals has shown single molecule Raman scattering cross sections that are orders of magnitude larger than free space single molecule luminescence cross sections. We analyze certain aspects of this phenomenon with new numerical electromagnetic calculations, and we also present new spectral depolarization data for single molecule rhodamine 6G scattering. We stress the central role of the Ag femtosecond radiative lifetime, and the spatial distribution of the excited Ag electrons, in the near field and far field optical properties. The fundamental nature of the Ag plasmon excited-electronic-state changes from a volume excitation to a surface junction excitation as two particles approach each other within 1 nm. Adsorbed molecules in the junction interact directly with the metallic excited-state wave function, showing electron-transfer-initiated photochemistry as well as enhanced Raman scattering. Depolarization studies show an uniaxial local electromagnetic symmetry at the junction site. Simultaneous intensity fluctuations in both the R6G molecular lines and the accompanying Ag electronic Raman continuum appear to reflect R6G adsorption−desorption kinetics. We outline the wavelength-dependent properties of a hybrid molecular-metallic wave function as the Raman resonant state.

1. Introduction

First observed in 1977, surface-enhanced Raman scattering (SERS) is a process in which the apparent Raman cross sections of molecules, adsorbed on roughened metal surfaces and particles, are enhanced on average by 5−6 orders of magnitude by local electromagnetic (EM) fields.[1−3] Approximately four thousand papers (many of these empirical analytical studies) have been published on SERS, yet the mechanism remains only qualitatively understood. This is in part because of the extreme heterogeneity and complexity of the surfaces, and in part because of fundamental spectroscopic issues. The invention of modern confocal single molecule techniques gives us new tools to unravel the complexity of SERS. With these methods Raman scattering from single dye molecules adsorbed on colloidal Ag nanoparticles was discovered to have enhancement factors of 10^{11} to 10^{12}.[4−9] *Under optimal conditions, when the molecule is also electronically resonant with the laser, the SERS Raman signal from a single molecule can be 10^2 to 10^3 stronger than a fully allowed, single molecule fluorescence signal in the absence of metal!* This remarkable development has opened opportunities for ultrasensitive analytical characterization (for a recent review, see ref 9), while at the same time it has renewed questions about the fundamental spectroscopic Hamiltonian.

Historically, SERS enhancement has been attributed to electromagnetic (EM) and "chemical" mechanisms.[1−3] The EM enhancement at the simplest level is due only to the special optical properties of the noble metals Ag, Au, and Cu—their ability to support surface plasmons at visible wavelengths—and not to the nature of the molecule. Surface plasmons greatly enhance the local EM field a few nanometers above the surface, resulting in increased Raman scattering. This model appears to be quantitatively correct for molecules not directly adsorbed on the metal.

However, molecular specificity in SERS does indicate the existence of a "chemical" effect for adsorbed molecules. For example, SERS scattering of adsorbed CO is almost 2 orders of magnitude stronger than that of N_2,[10] though they have nearly identical free space Raman cross sections. In addition, the SERS cross section for pyridine adsorbed onto rough Ag electrodes depends on the applied voltage.[3] Accordingly, models describing the molecule−metal charge-transfer interaction, where an electron is transferred from the molecule HOMO to the metal or from the metal to the molecule LUMO, have been proposed to explain some aspects of the "chemical" effect.[2,3,11] As a result, SERS may come from a resonant scattering process of the molecule−metal charge-transfer complex. As we shall argue in this paper, this "chemical" effect is a microscopic quantum mechanical aspect of EM enhancement, not a fundamentally different mechanism.

Previously, we reported huge SERS cross sections (∼200 Å^2), including both vibrational Raman lines and a broad underlying continuum, for single rhodamine 6G (R6G) molecules adsorbed on Ag nanocrystal aggregates.[6] Only fewer than 1% of the Ag particles give detectable SERS activity. Far field resonant Rayleigh scattering spectra have been correlated with SERS to probe the EM enhancement, together with the atomic force microscopy (AFM) study of the morphology of the SERS active "hot particles".[6,12] Our results show that all "hot particles" are compact, nonfractal aggregates of Ag nanoparticles. We assigned the SERS single molecule "hot spots" as the junctions between nanoparticles, on the basis of our data and the 1983 theoretical calculations of Inoue and Ohtaka.[13] In the similar system of hemoglobin/Ag colloid single molecule SERS, strong evidence

10.1021/jp034632u CCC: $25.00
Published on Web 08/20/2003

for junction sites was independently obtained by Xu, Bjerneld, Kall, and Borjesson.[7]

In this paper we report new results and calculations, and we explore in more detail the issues and unsolved problems associated with this giant EM SERS effect at junction sites. We still do not know how to quantitatively analyze and predict this molecular scattering process. In section 2, we discuss how classical EM enhancement depends on shape, size, and aggregation, as well as how excited electronic states in metallic particles create local EM fields. In section 3 we discuss the broader question of molecular photochemistry on metal particle surfaces. In section 4 we explore, and present new data on, the symmetry of the excited-state wave function as revealed by Raman depolarization studies as a function of wavelength. Earlier we had shown that the typical molecule which gives rise to an intense single molecule SERS signal sits in an extremely anisotropic local EM environment.[14] Finally, we discuss the quantum mechanics of this process.

2. Classical Electromagnetic Field Enhancement

Strongly enhanced local EM fields are due to plasmon excitation by incident plane wave light. On the flat surface of a bulk metal, surface plasmon excitation is forbidden by momentum conservation in the plane of the surface; flat surfaces show only very weak SERS.[15,16] On rough surfaces this conservation rule is broken. In the case of particles, plasmons interact with incident plane wave light as determined by their dipole (and higher multipole) transition moments, which depend both upon shape and size with respect to the optical wavelength and upon the nature of the material.

For spherical particles with diameter less than the wavelength of incident radiation, the problem can be solved by standard electrostatics. Here we discuss certain aspects and present new numerical calculations for EM field enhancement for a single sphere, and a dimer of spheres as a function of their separation.

Isolated Single Metal Sphere. An isolated material sphere of radius R and complex, wavelength-dependent dielectric constant $\epsilon = \epsilon' + i\epsilon''$, when placed in a plane wave EM field, will develop an internal polarization **P(r)** [ac dipole moment per unit volume, sometimes called "optical currents"], oscillating coherently with respect to the driving field $\mathbf{E_0}$. The external EM field collectively created by this internal polarization can be represented by the field of a point dipole **p** located at the sphere center, which scales with sphere volume as

$$\mathbf{p} = 4\pi\epsilon_0\epsilon_m\left(\frac{\epsilon - \epsilon_m}{\epsilon + 2\epsilon_m}\right)R^3\mathbf{E_0} \qquad (1)$$

ϵ_m is the dielectric constant of the surrounding medium, and ϵ_0 is the permittivity of the vacuum. In the electrostatic limit without retardation,[17] **P(r)** is related to the local internal electric field strength $\mathbf{E_{in}(r)}$ and the incident field $\mathbf{E_0}$ by

$$\mathbf{P(r)} = \epsilon_0(\epsilon - \epsilon_m)\mathbf{E_{in}(r)} = 3\epsilon_0\epsilon_m\left(\frac{\epsilon - \epsilon_m}{\epsilon + 2\epsilon_m}\right)\mathbf{E_0} \qquad (2)$$

P and $\mathbf{E_{in}}$ are independent of **r** within isolated spheres. As a sphere grows in size, **p** increases, but so does the distance of a surface molecule from **p**. The net effect is constant surface field enhancement.

The EM field outside the particle is a superposition of the incident field $\mathbf{E_0}$ and the dipole field due to **p**. Along the particle axis (defined as the incident electric field direction) just above the surface, this local field is maximum and given by

$$\mathbf{E_{surf}} = \frac{3\epsilon}{\epsilon + 2\epsilon_m}\mathbf{E_0} \qquad (3)$$

independent of radius R. At the dipolar plasmon resonance wavelength, by definition where the real part of the complex dielectric constant ϵ' approaches -2, the electric field inside and outside the particle will be very large. The magnitude depends on the imaginary part of the complex dielectric constant ϵ''. Note that if all surfaces of a particle are simultaneously irradiated with an EM field, then there is no distinction between bulk and surface plasmons. Instead, plasmons are defined by their local mode symmetries.

Noble metals, such as Ag, Au, and Cu, have dipolar plasmon frequencies with fairly small ϵ'' compared to those of other materials, and thus have large internal fields. Normally both incident and scattered local fields lie in the plasmon enhancement region; thus, the apparent Raman cross section is approximately proportional to the fourth power of the enhanced local field. This electromagnetic field enhancement from a single particle can account for a 10^6 enhancement factor averaged over the surface. This plasmon SERS model was first suggested independently by Moskovits[18] and Creighton et al.[19] and developed by Kerker et al.[20] If we neglect the dependence of the dielectric constant upon particle size, this model predicts constant enhancement independent of size, for small particles much less than the wavelength in diameter. As size approaches the wavelength, destructive interference from retardation causes the surface enhancement to diminish and shift to longer wavelength.[20]

At a given irradiation wavelength λ, the local field intensity near metal sphere surfaces is related to the induced dipole **p**, which also determines the sphere absorption and Rayleigh scattering cross sections. For diameters much less than λ the cross sections are

$$\sigma_{abs} = \frac{8\pi^2R^3\sqrt{\epsilon_m}}{\lambda}\left|\mathrm{Im}\left(\frac{\epsilon - \epsilon_m}{\epsilon + 2\epsilon_m}\right)\right| = \frac{2\pi}{\lambda\epsilon_0\sqrt{\epsilon_m}}\left|\mathrm{Im}\,\frac{\mathbf{p}}{\mathbf{E_0}}\right| \qquad (4)$$

and

$$\sigma_{sca} = \frac{128\pi^5R^6\epsilon_m^2}{3\lambda^4}\left|\frac{\epsilon - \epsilon_m}{\epsilon + 2\epsilon_m}\right|^2 = \frac{8\pi^3}{3\lambda^4\epsilon_0^2}\frac{\mathbf{p}^2}{\mathbf{E_0^2}} \qquad (5)$$

The plasmon creates the same resonant peak wavelength in both cross sections, as well as in the local field intensity. For small particles, the absorption, proportional to the particle volume, dominates the extinction. As particle volume increases, the scattering, which scales as R^6, takes over eventually. For silver particles, scattering starts to dominate the extinction efficiency with $R > 20$ nm.[21]

For particles of 2−4 nm diameter, the effective dielectric constant becomes size and surface dependent because the particle diameter is less than the electron mean free path.[22] For a given size, this additional broadening sensitively depends on surface roughness and the chemical nature of the adsorbed species. Due to this surface scattering damping effect, the homogeneous plasmon bandwidth, Γ_{hom}, in the two cross sections above, increases, while the enhanced local field strength, which is inversely proportional to Γ_{hom}, decreases.[23]

The giant SERS effect is observed in aggregates of larger, 30−60 nm, particles. At this size, retardation and higher order plasmon modes create further plasmon band broadening, and

EM enhancement in single particles decreases. In addition, damping due to Rayleigh reradiation into the far field becomes significant. Taking into account surface scattering, retardation, multipole plasmon excitations, and radiation damping, the highest Raman enhancement factor for single Ag spheres was found for particles with 20−25 nm radius.[21,24] Furthermore, as particle size increases, the wavelength dependencies of near field and far field scattering do not peak at the same frequency. A molecule placed near or on a metal particle surface experiences a strongly enhanced or weakly enhanced local field depending upon the position on the sphere.[25] The local electric field at different positions has different wavelength dispersions, which also differ from the far field extinction dispersion curve.

Various shapes of nanoparticles,[26,27] cavity sites between particles,[28,29] and sharp points or protrusions on the particle[30] have been incorporated into the electromagnetic field enhancement calculations. Spheroids, in particular, for their simplicity, have been extensively calculated.[31−33] Results have shown that electric fields at locations associated with high curvature features (spheroid tips) are higher than the spherical particle case, and the enhancement factor increases as the aspect ratio of the spheroid increases, which is sometimes referred to as the "lightning rod" effect.

In general, **p** gives the scattering rate of incident plane-wave light in a photostationary metallic particle excited electronic state. The magnitude of **p** and the level of excitation depend both upon the intensity of the exciting EM field and upon the rate of internal radiationless decay producing heat in the particle, as embodied in the imaginary part of the bulk dielectric coefficient and possible additional surface scattering. The plasmon is an excited electronic state of the metallic particle and, when coupled to the EM field, simultaneously a local "polariton" mode of this field. This local mode can contain more than one quantum of energy. The plasmon model assumes a negligible change in electronic structure in the excited state, which thus interacts with the EM field in exactly the same fashion as the ground state. That is, there is no saturation or nonlinearity as the driving field is increased in strength. In contrast, molecules change their electronic structure (and often geometry) upon excitation, and thus the excited state interacts with the EM field differently. To make a comparison with molecules, we can ask what is the decay lifetime of an excited plasmon state whose spatially integrated local EM field due to **p** has one quantum of energy. This lifetime shortens with increasing size and is on the order of 10 fs for $d = 200$ nm.[34] For such large Ag particles it is a purely radiative lifetime; almost all the initial near field energy radiates away into the far field,[35] as is also implied by the fact that the scattering cross section is much larger than the absorption cross section. A high oscillator strength necessarily implies a high scattering cross section. *Such large Ag particles act as almost ideal microscopic antennas; they concentrate the EM energy in a subwavelength region without significant dissipation into heat.*

The huge oscillator strength of the dipole **p** associated with a 10 fs radiative lifetime is the source of the SERS effect. When this huge dipole is coupled to the EM field, it changes the field structure and creates a local "polariton" field mode. By contrast, molecules have purely radiative lifetimes no shorter than ∼1 ns due to their small size. This dipole is too small to change the EM field structure.

Aggregated Metal Particles. Calculations on larger aggregates show that the essential new feature is present in the two-sphere dimer model,[13] which itself has been approached by various groups using different methods.[30,36−38] The electromagnetic field in the particle junction midway between the spheres is not a simple coherent sum of the fields from the individual particles. Instead, as the particles approach, there is a dramatic enhancement increase. As we show below, this is due to coherent capacitive coupling between particles profoundly changing **P(r)** in each particle. Heuristically, the **p** near field of one particle induces quadrupolar and higher order moments in the close neighbor particle, and this likewise mutual induction produces an infinite sum of coherently oscillating higher order multipole moments. (These higher moments are defined for expansion about the two particle centers; however, if **P(r)** is expanded about the midway junction point, then the combined interacting polarizations remain mainly a dipole moment.) This hierarchy of multipoles is apparent in the work of Xu and Dingham.[39] The near fields of all these moments coherently add to produce maximum external field enhancement in the junction. The Raman enhancement factor can be 10^{10} to 10^{12} for a separation of 1 nm. This enormously enhanced field is highly localized in a few cubic nanometers; it is an ideal situation for single molecule Raman spectroscopy, as only a few molecules can fit into this "hot spot".

With 2.5 eV (497 nm) excitation, polarized along the line of centers of two 60 nm diameter Ag spheres, the Raman enhancement factor at the midpoint of the two-particles junction increases from 1.5×10^4 to 5.5×10^9, when the particle gap shrinks from 9 to 1 nm. The coupling between two spheres is quite short-ranged, as the enhancement is only 8.4 at particle separation on the order of particle diameter or larger.

This huge enhancement occurs for particles of optimized size. For a fixed particle surface-to-surface separation, the enhancement grows with increasing particle diameter and reaches maximum magnitude when retardation begins to affect the phasing of the fields and when the combined **P(r)** begins to develop a substantial quadrupole moment about the junction. In a heuristic sense, the junction enhancement grows with size because the ac current density passing through the junction increases with Ag volume. For visible light (514.5 nm) this maximum diameter is about 90 nm for Ag,[7] that is, 180 nm total length. For single spheres, as discussed earlier, the (smaller) enhancement is the largest when particle diameter is about 40 nm irrespective of the wavelength.[30] If one made a SERS junction from two touching semi-infinite local probe metallic tips, the junction enhancement would be lower, and the Rayleigh scattering (which interferes with sensitive Raman detection) would be far higher. This finite optimized size effect is also known in the design of single particle apertureless near field probes.[40]

The limited spatial extent of the enhanced electric field creates a high EM gradient at the junction,[30] which must change the Raman scattering Hamiltonian, as compared with normal Raman scattering in free space. Owing to the polarization coupling effect, and unlike the single sphere case, field enhancement will strongly depend on the incident field polarization direction. If the field is polarized along the dimer axis, then the enhancement reaches maximum. It drops significantly when field is polarized along the transverse direction. This crudely resembles the excitation of the longitudinal and transverse modes in a spheroid.

P(r) Distributions. To obtain the **P(r)** spatial distribution, and to understand the Raman junction effect in different materials, we numerically calculate **P(*z*)** directly along the line of centers (*z* axis), following Aravind et al.'s method.[36] By choosing bispherical coordinates and neglecting retardation, the Laplace equation can be solved with the boundary conditions that potential and the electric displacement normal across two

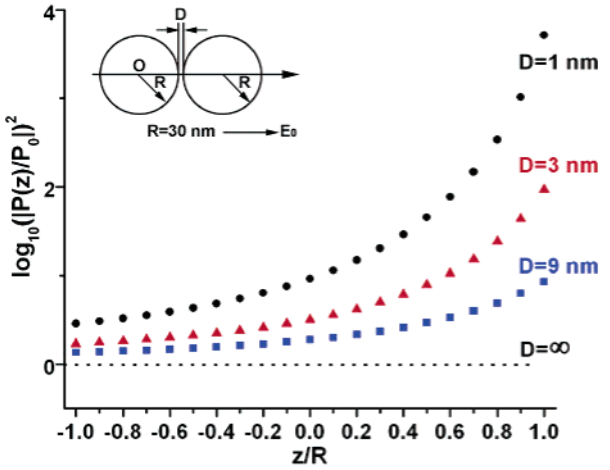

Figure 1. Changes of the metal excited-state density distribution of the two-particle system (configuration shown in the inset) compared to the single-particle case, as a function of particle coupling. $z/R = 0$ is at one particle center, and $z/R = +1$ is on the particle surface at the particle−particle interface side.

TABLE 1: Raman Enhancement at the Midpoint of the Two 60 nm Diameter Spherical Particle Junction for Various Materials and Separations with an Excitation Laser of 2.5 eV (497 nm)

	Ag	Al	Si	SiO_2
1 nm	5.5×10^9	5.0×10^6	1.0×10^5	8.8×10^1
3 nm	1.7×10^6	8.4×10^4	8.9×10^3	4.9×10^1
9 nm	1.5×10^4	3.0×10^3	7.3×10^2	2.1×10^1

media are continuous. The internal electric field $\mathbf{E_{in}}(z)$ is obtained as a function of excitation wavelength, excitation angle, and interparticle distance. For large particles we use the bulk optical dielectric data.[41] $\mathbf{P}(z)$ is obtained as $\mathbf{P}(z) = \epsilon_0(\epsilon - \epsilon_m)\mathbf{E_{in}}(z)$.

For single spheres, $\mathbf{P}(z)$ is constant across the particle diameter. In Figure 1, $\mathbf{P}(z)$ for the dimer is pulled into the interparticle interface region and reaches the maximum on the interface as the particles approach. In this figure the origin is set at one sphere center, $z/R = +1$ corresponds to the particle surface at the junction, and $\mathbf{P}(z)$ is normalized to its single sphere value. This capacitive coupling of one Ag particle to the other draws the metallic excited electronic state represented by $\mathbf{P}(z)$ into the junction. By Gauss's law, this surface polarization creates the high field in the junction. The falloff rate of $\mathbf{P}(z)$ dramatically increases as interparticle separation shrinks. This rate can be parametrized by defining the decay length L of $|\mathbf{P}|^2$ as the position where $|\mathbf{P}|^2$ drops to 1/e of the surface value. With 2.5 eV laser excitation of 60 nm diameter Ag particles, L is 1.7 nm at 1 nm separation but increases to 18 nm for 9 nm separation, almost equal to the particle radius.

This huge field enhancement effect is due to the Ag plasmon resonance. Ag has very small damping (imaginary part of the dielectric constant ϵ'') at the surface plasmon resonance. Au and Cu are similar to Ag but have larger damping constants. For comparison, we have also calculated Al, Si, and SiO_2 as typical examples for metal, semiconductor, and insulator. Optical constants for them are taken from the literature.[42] Calculated Raman enhancement factors, $|\mathbf{E}/\mathbf{E_0}|$,[4] due to the enhanced EM field in the middle of the junction are tabulated in Table 1 for 60 nm diameter particles excited at 2.5 eV (497 nm), separated by 1, 3, and 9 nm, respectively. The field enhancement decreases in the order Ag, Al, Si, and SiO_2, and the difference is much more dramatic at closer distances. Tian et al.[43] have done SERS on transition metal surfaces, but with very weak enhancement. Exceptions are alkali metals. In theory, they are also very good substrates for surface enhancement, but their use is hindered by their extremely high chemical activity.

Microscopic Nature of P(r). Microscopically, **P(r)** represents coherently oscillating, optically driven ballistic electron−hole pairs, as Kubo described.[44] These ballistic pairs can either reradiate at the laser frequency (Rayleigh scattering) or relax, producing heat. $|\mathbf{P}(\mathbf{r})|^2$ is proportional to the spatial probability density of the excited state created by continuous excitation at the wavelength λ. *Because metals are so polarizable, the fundamental nature of the metallic excited state* $|\mathbf{P}(\mathbf{r})|^2$ *changes from a volume excitation to a surface excitation as two particles approach.* The metal surfaces in the junction, where $|\mathbf{P}(\mathbf{r})|^2$ is high, experience alternating fluxes of ballistic electrons and holes, along z, every half of the optical cycle. Molecules adsorbed on the metal surface in the junction can interact directly with $|\mathbf{P}(\mathbf{r})|^2$ via electron exchange and with the enhanced EM field in the junction. In fact, as we observed in a previous publication,[12] Gauss's law requires that the surface value of $|\mathbf{P}(\mathbf{r})|^2$ scale exactly with the enhanced field above that surface in the junction. A consequence is that the vast literature of enhanced EM field calculations should be good indicators of the spatial position of the maximum SERS effect, regardless of the true form of the spectroscopic Hamiltonian.

3. Surface Adsorption, Photochemistry, and SERS Activity

Adsorbed molecules can interact with the excited metallic electrons $|\mathbf{P}(\mathbf{r})|^2$ on the surface, as well as with the enhanced field above the surface. Even physisorbed molecules can have a significant electron exchange interaction with the metallic s−p electrons that spill out from the surface. For example, high vacuum photoelectron and Kelvin probe studies of C_{60} on flat terraces of Au and Ag show strong interfacial dipoles due to repulsive Born exchange; these dipoles point in the opposite direction to that for dipoles due to metal to C_{60} charge transfer.[45,46] These dipoles produce local work function changes and are present even in the case of adsorbed xenon.[47] The strength of the calculated adsorbate−metal dipole moments correlates with an adsorbate's ability to quench optically created hot electrons in laser studies.[48] This quenching corresponds to the adsorbate induced plasmon spectral broadening mentioned previously.

Photochemistry due to direct molecular excitation on metal surfaces is normally quenched by the extremely fast rate of molecular excited-state energy transfer into the metal.[49] In fact, this fast energy transfer is an essential element of single molecule sensitivity in our adsorbed R6G case, as it quenches excited-state R6G luminescence that would otherwise interfere with Raman scattering.

However, in some cases adsorbed molecules undergo photochemistry due to optical excitation of the metallic electrons, in addition to undergoing SERS. The exchange and charge-transfer surface electronic processes postulated for chemical SERS[2,50,51] activation are closely related to the known electrochemical reactivity and photoreactivity of silver nanocrystals, as shown by the pioneering work of Henglein[52−57] and others.[58−63] These effects are enhanced by nanometric dispersion of the silver particles, creating a large surface-to-volume ratio. Adsorbed nucleophilic molecules such as cyanide ions[56] and phosphine[64] show clear charge-transfer effects on noble metal nanocrystals. The Fermi level of silver exhibits a shift proportional to the partial charge involved in the molecule adsorption

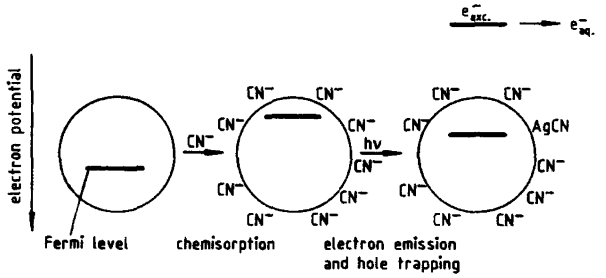

Figure 2. Schematic description of silver photoelectron emission and surface atom oxidation in illuminated silver particles precomplexed by cyanide ions. The shift of the Fermi level in the particle is also indicated (Reprinted with permission from ref 56. Copyright 1991).

and inversely proportional to the particle size. This adsorption-induced polarization of the interface has a similar effect to that of an applied voltage on an electrode. In terms of reactivity, the redox potentials approach each other:[54] silver becomes easier to oxidize and the adsorbate becomes easier to reduce. Such nanoparticles behave as electron-transfer catalysts if the silver potential is between the molecular oxidation and reduction potentials of two different adsorbed species.[53,63] In terms of molecules, this strong interaction between a molecule and a silver nanoparticle can be described by the formation of a "precomplex", formed by the adsorbed molecule bounded to a "preoxidized" silver adatom.[56]

Despite the femtosecond time scale of electron−hole $|\mathbf{P(r)}|^2$ recombination in metals, adsorbed molecules can undergo photoinitiated electron-transfer processes. The photoreduction of methyl viologen on silver nanoparticles[62] and the photo-oxidation of silver by cyanide ions[56] are examples. In the latter case, the process follows Henglein's mechanism in Figure 2. Adsorption of cyanide induces a charge transfer and a shift of the Fermi level. Because of that, absorption of a photon induces the photolysis of silver, forming an AgCN complex molecule with the ejection of an electron into the solution. The measured quantum yield is about 1% for irradiation in the ultraviolet near 300 nm wavelength.

Such surface photochemistry, even at low laser power, can complicate SERS as new species are created. For example, in a single molecule SERS study of tyrosine, which is optically transparent at the laser wavelength 514.5 nm, it was found that the observed strong signals came from unidentified resonant transient species produced in a linear photoprocess.[65] In studies of hemoglobin single molecule SERS in aggregated Ag colloids, the extent of photochemical transformation remains an open question.[7] In ensemble studies, Moskovits and co-workers have observed photodecomposition and photodesorption reactions for adsorbed SERS molecules such as azabenzenes and 2-amino-pyridine.[66−68] An initial charge-transfer optical excitation is often postulated in these experiments. Also, amorphous carbon-like spectra have been observed by SERS in a number of experiments as final products at higher laser power.

4. Single Molecule Fluctuation and Local Symmetry in Compact SERS Aggregates

Figure 3 shows a typical compact aggregate with its white light Rayleigh scattering and single molecule R6G SERS spectra. The Rayleigh spectrum is complex and broad, as expected from several strongly coupled nanocrystal scatterers. The Raman spectrum shows a broad underlying continuum as well as sharp R6G Raman lines. We now describe spectrally resolved Raman depolarization studies on such stationary aggregates.

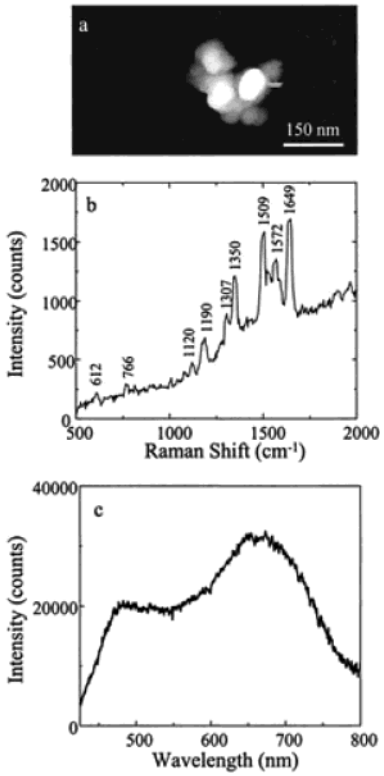

Figure 3. (a) AFM image, (b) R6G SERS spectrum, and (c) resonant Rayleigh scattering spectrum of a single SERS-active Ag particle incubated with 10 mM NaCl and 2 nM R6G. For the SERS spectrum, the integration time was 60 s at ~30 W/cm^2. The Rayleigh scattering spectrum was obtained with a 10 s integration time (Reprinted with permission from ref 12. Copyright 2000 American Chemical Society).

Depolarization studies reveal spatial symmetry and possible molecular rotational averaging in the Raman scattering process. This is an important issue in single molecule SERS, which is complicated by strong intensity fluctuations (and blinking) for fixed incident and scattering angles. In single molecule studies, fluctuations indicate molecular dipolar orientational motion or a kinetic process such as photoionization or desorption that might change the absolute Raman cross section. Depolarization measurements, which compare the simultaneously recorded s- and p-polarized signals, help to distinguish these issues. In a previous publication[14] we investigated these fluctuation and local symmetry issues for the entire spectrally integrated (continuum plus Raman lines) Stokes SERS at 514.5 nm. While the unpolarized Stokes intensity fluctuated quite dramatically on a time scale of seconds, the depolarization ratio $\rho = (I_{ss} - I_{sp})/(I_{ss} + I_{sp})$ was time-independent. This effect is ascribed to the depolarization ratio being controlled solely by the anisotropic enhanced field in just one internal junction in the aggregate.

The sharp R6G Raman lines typically constitute 10% of the integrated SERS Stokes intensity. The prior studies thus only measured continuum depolarization. We now report ρ as a function of λ for both Raman lines and the continuum. Hildebrandt and Stockburger observed in 1984[69] that the excitation profile of ensemble R6G SERS peaks at the molecular resonance near 530 nm. Careful measurements by Weiss and Haran,[8] using 532 nm laser excitation, yield a higher Raman cross section for single R6G adsorbed on Ag nanocrystals compared to that found using 514.5 nm excitation, in rough agreement with the ensemble studies. We use 528.7 nm (Ar ion laser Coherent Innova 308) where our signal is about 3−5 times stronger than that at 514.5 nm.

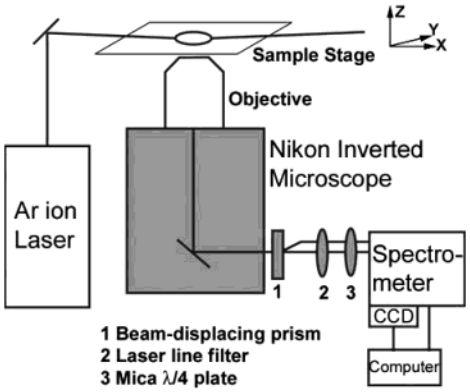

Figure 4. Schematics of the experimental setup. s- and p-scattered light is displaced by a beam displacing prism and simultaneously recorded on a CCD camera.

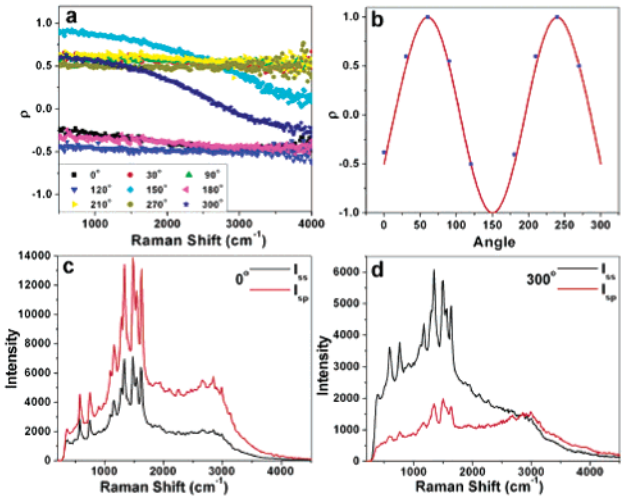

Figure 5. Simultaneous measurement of s- and p-polarized SERS signals from a single R6G molecule on an Ag aggregate. 528.7 nm laser excitation was used with a fixed intensity of ~80 W/cm^2. (a) Raman shift dispersion of polarization parameter ρ (see text) at various rotation angles. (b) Averaged ρ at various angles fitted with a cos(2θ) curve. (c and d) Raman spectra for the two different behaviors, constant ρ and varying ρ as a function of Raman shift, respectively.

As shown in Figure 4, s- and p-polarized stokes-shifted light, separated by a beam displacing prism (Melles Griot), were collected simultaneously from one aggregate. Laser polarization was fixed in the *XY* plane, while the sample orientation can be changed by rotating through angle θ about *Z* perpendicular to the *XY* plane. For most aggregates, ρ is constant across the spectrum and varies strongly when rotating the sample stage. The spectra of I_{ss} and I_{sp} have been recorded simultaneously for sequential 1 s integrations for a few intense SERS-active spots at higher laser intensity (~230 W/cm^2). Both s and p SERS spectra have the same relative proportions of R6G Raman lines and background continuum, and they fluctuate together, as previously observed by Weiss and Haran for combined s and p spectra.[8]

At 80 W/cm^2 and 60 s integration, Figure 5c shows typical s and p spectra for a fixed angle θ. Before one complete 360° rotation with 30° steps could be completed in this case, the SERS signal was lost due to photobleaching. For this aggregate ρ is constant across the spectrum, as shown in Figure 5a, except at 150° and 300°, where depolarization ratios show some fluctuation behavior. At the angles 60° and 240°, the p-polarized Raman scattering component vanishes; thus, ρ is +1. In Figure 5b, the averaged depolarization ratios are compared with a cos(2θ) curve. In the 300° abnormal fluctuation data (Figure 5d),

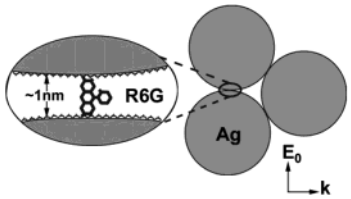

Figure 6. Schematic representation of SERS active aggregate geometry. A single R6G molecule adsorbed on the Ag particle covered with a citrate layer. The xanthene plane is aligned along the local field direction.

it appears that this aggregate briefly developed a second broad continuum feature near 3000 cm^{-1}, perhaps at another location in the aggregate with a different depolarization ratio.

While there are a few cases where ρ was constant at all angles, for most cases the cos(2θ) curve is observed. As previously discussed,[14] this depolarization effect is expected if the R6G molecule is permanently located in one junction, and both excitation and Stokes radiating dipoles are along the local enhanced field—the line of centers of the two touching particles. More generally, a cos(2θ) depolarization ratio is expected for a single (i.e., not spatially degenerate and not rotationally averaged) dipole attached to the substrate and rotating about *Z* with the substrate. Figure 6 shows a simple aggregate with three separate junctions, each of which would give a cos(2θ) curve maximizing at different angles. There is also a central more symmetric cavity site which would show a different depolarization behavior. The uniaxial symmetry of the junction site creates a substantially depolarized Raman signal when averaged over all incident angles, even for totally symmetric molecular modes. This result helps us to understand the Raman depolarization commonly observed in early ensemble studies.

Thus, both sharp Raman lines and the continuum originate in one anisotropic junction with dipoles pointing in the same direction. They also fluctuate together. Taken together, this is strong evidence that both Stokes components are triggered by one R6G that experiences one local field at a fixed place in the aggregate. For R6G to undergo a strong molecular resonance Raman enhancement, the EM field must be parallel to the long xanthene aromatic axis, as this is the direction of the $\pi-\pi^*$ transition dipole. This suggests R6G is adsorbed standing up in the citrate layer—if it were flat on the surface, we would not see molecular resonance at 530 nm excitation. It is thought that R6G makes a polar bond with the Ag surface via N^+ at one end of the xanthene group,[70] consistent with the observation of the Ag−N stretch in the ensemble SERS spectra.[69] The dipole direction of the oscillating electron−hole pairs is also perpendicular to the surface; this would be the dipole for the electronic Raman continuum discussed in the next section.

The observed fluctuations represent changes in absolute cross section, not tensor properties. We assign the fluctuations, as do Weiss and Haran, to changes in the strength of adsorption. These authors showed that coadsorption of Cl^- influences the fluctuation behavior, an effect that they attribute to screening of local static electric fields (from areas of differing local work functions) that influence surface mobility.[8]

5. SERS Continuum and Electronic Raman Continuum

As has been noted since the early days of SERS, the vibrational Raman lines are always accompanied by continuous scattering, often conjectured to be luminescence[71] or electronic Raman scattering[72,73] from the underlying metal. In ensemble studies, the continuum is observed even for molecules that are transparent (i.e., do not absorb or luminescence) at the laser

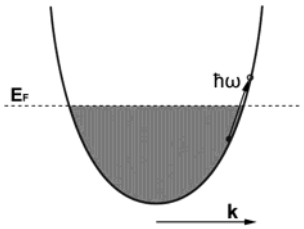

Figure 7. Schematic illustration of the Ag conduction band structure.

frequency, such as pyridine molecules or CN^- ions on an electrically roughened Ag electrode.[71,72] The continuum is an aspect of SERS not present in normal free space molecular Raman scattering.

Electronic Raman scattering is an inelastic photon scattering process that creates an electron−hole pair in the metal; that is, it excites an electron from below to above the Fermi surface. In crystalline metals such as Ag, which can be understood as a simple isotropic Fermi liquid with a well defined electronic momentum *k*, electronic Raman scattering is normally very weak because *Q*, the photon momentum transferred to the electron−hole pair, is only large enough to create an electron−hole pair of a few inverse centimeters energy above the Fermi surface. For a typical photon in the visible ($\lambda \sim 500$ nm) and 90° scattering geometry, the transferred momentum is on the order of 10^{-3} Å^{-1}. Compared to the lattice constant of a typical crystal of 4 Å, practically no momentum transfer happens in the light scattering process. This can be schematically illustrated by Figure 7. However, in "dirty metals" the *k* selection rules are relaxed by scattering off defects, and electronic Raman scattering over a wide energy range becomes possible.[74−76] Thus, strong electronic Raman scattering in Ag is associated with defects, on rough, cold deposited Ag films[77,78] and on the surfaces of Ag nanocrystals formed by ion implantation into silica.[79]

Our 50 nm Ag nanocrystals grow and anneal at 100 °C, in refluxing water and in a reducing citrate environment.[80] They show faceted shapes at high TEM resolution. They are high quality single Ag nanocrystals without surface oxide and covered with an adsorbed hydroscopic citrate layer. In the Stokes screening experiment, single particles and aggregates do not show Ag electronic Raman scattering or vibrational citrate Raman scattering before R6G adsorption. Heuristically, the absence of electronic Raman scattering implies their surfaces are "smooth" without defects or adatoms; electrons undergo specular reflection (without dephasing) at their surfaces, as also occurs on flat clean single crystal Ag surfaces in high vacuum. The nonresonant citrate ions do not interact strongly enough with the Ag electron−hole pairs created at 514.5 nm to act as a "defect".

However, when R6G is present in the junction site, we see both continuum and R6G vibrational lines with a huge net cross section and the same depolarization ratio. Moreover, we see these signal blink on and off together[6] and fluctuate together.[8] The simplest assumption is that the continuum is Ag electronic Raman scattering caused by just one surface defect−an adsorbed R6G exchanging electrons with the metal. Scattering of the coherently driven plasmon surface $|\mathbf{P(r)}|^2$ electrons off this adsorbed molecule creates both R6G first layer SERS and Ag electronic Raman scattering.

6. Outline of a Possible Metal−Molecule Resonant State

The free space Kramers−Heisenberg−Dirac Raman scattering cross section σ, between the initial state i and the final state f, is proportional to

$$\left| \sum_r \frac{\langle f|\mu|r\rangle\langle r|\mu|i\rangle}{E_{ri} - \hbar\omega + i\Gamma} > \right|^2 \quad (6)$$

where the summation is over all excited states *r* at different energies.[81] In resonance Raman scattering, one excited state dominates this sum. This formula includes only dipole (μ) interaction terms; possible $\nabla\cdot\mathbf{A}$ terms (**A** is the EM field vector potential) are ignored because the EM wavelength is much larger than the molecule. However, a molecule in a junction of width 1 nm between two Ag nanocrystals of ∼50 nm diameter sees a classical EM field that varies on the same length scale as the molecule itself. Inside the nanocrystals the plasmon local EM mode is an optical current (ac polarization) represented by $|\mathbf{P(r)}|^2$. As the electrons spill out of the surface of one nanocrystal into the junction, the local EM mode changes into an enhanced EM field for a few angstroms and then changes back into an ac current in the other nanocrystal. In surface photoemission experiments on metals, the $\nabla\cdot\mathbf{A}$ term is known to modify the normal bulk dipole formulas.[82,83] In the ensemble SERS of high symmetry aromatic molecules, the appearance of normally forbidden modes has been attributed to this term.[84] This effect should be significant inside the SERS junction. The simple free space scattering formulas must be modified if the enhanced surface EM field concept is to be retained. Even if this problem is understood, the EM field magnitude and distribution in the 1 nm junction need to be calculated using a nonlocal Ag dielectric response model with accurate surface screening.[85] Early SERS workers recognized both of these problems in the context of rough surfaces, as discussed in the Moskovits review. Both problems remain unsolved today.

Adsorbed molecules are coupled to the metal by electron exchange, and the metallic particle itself is resonant with the laser. Thus, heuristically we might explore a metal−molecule resonance Raman model and try to ignore the concept of enhanced surface EM field. Molecule−metallic cluster SERS prototypes (without junctions), such as $Ag_{10}CO$, have been explored by numerical electronic structure calculations and show a very strong (10^7 increase) CO vibration resonance Raman effect[86] derived from the oscillator strength of a Ag_{10} excited electronic state. This calculation shows the essence of the SERS mechanism for adsorbed molecules. However, large systems are far beyond the present numerical calculations.

In our R6G experiments, the 514.5 nm (or 528.7 nm) excitation is resonant with an R6G electronic transition, such that our measured cross section includes a contribution from the R6G excited-state resonance Raman effect. A metal−molecule resonant excited state should include an exchange coupled molecular excited-state contribution. Any metal−molecule resonant state must also include possible charge-transfer "chemical" enhancement terms. In the early days of SERS, Lombardi[11] and Creighton[87] independently introduced physically reasonable charge-transfer Raman models to explain chemical effects. In these theories, the charge-transfer transition creates a molecular resonance that increases the molecular Raman cross section at that laser wavelength. The normal local EM field enhancement factor then multiplies this enlarged Raman molecular cross section.

In the ideal many body electron sea of a metal, collective plasmon excited states exist in addition to simple, molecular-like single particle states. The plasmon excited state in the random phase approximation is a coherent superposition of low energy electron and hole states near the Fermi level.[88] By coherent evolution (termed Landau damping) this nonstationary collective state decays into single electron−hole pair excitations

degenerate with the laser energy.[89] At fixed frequency, steady-state irradiation, this is the type of coherent electron−hole pair that creates **P(r)** "optical currents" in the metal. In molecular spectroscopy, this evolution is somewhat analogous to the nonstationary first excited singlet state of a molecule decaying into high lying vibrational levels of the ground state.

In 1983 Persson outlined a schematic resonance Raman SERS spectroscopic Hamiltonian based upon the charge-transfer terms in the Anderson−Newns chemisorption Hamiltonian.[50] This model has been discussed in depth with respect to single molecule SERS by Otto.[78] More generally, such a metal−molecule resonant state should include exchange coupled metallic excitations, charge-transfer excitations, and molecular electronic excitations. This can be formally written as

$$\left\{ \sum_{k<k_F,q} a_{kq} c^{+}_{k+q} c_k + \sum_q (a^{L}_q c^{+}_{L} c_{k_L-q} + a^{H}_q c^{+}_{k_{H+q}} c_H) + a^{LH} c^{+}_{L} c_H \right\} |0\rangle \quad (7)$$

where all four terms represent different types of neutral excitations. The first term represents all possible surface electron−hole pairs made by Landau decay of the plasmon; this corresponds to the macroscopic $|\mathbf{P(r)}|^2$. The energy of each individual pair is the laser energy. The last term is the molecular HOMO−LUMO excited state of fixed energy. When the laser is off the molecular resonance, the exchange coupled admixture of this term in (7) is small; on resonance it is larger. The second and third terms are charge-transfer excitations in both directions at the interface. The c's and c^+'s are annihilation and creation operators for electrons, and the a's are expansion coefficients. L and H refer to the molecular LUMO and HOMO, and the k's refer to the metal electron states; k_L and k_H refer to metal electron states degenerate with the LUMO and HOMO. This wave function is obviously completely coherent. Substitution of the wave function into (6) as the resonant state would give the effective SERS cross section. Note that this picture makes it obvious that the enhancement applies to both the incoming and outgoing photons.

The relative proportions of the four terms in (7) should vary as the laser wavelength is scanned. Also, for fixed laser frequency, the relative proportions of the two charge-transfer terms would vary with changes in the local work function at the R6G site, for example, on a flat terrace versus a step edge, or with local coadsorption of small species such as O_2 or Cl^-. Our case of adsorbed R6G would be a case where the fourth term determines the high frequency aromatic stretch resonance conditions; Weiss and Haran[8] have argued that the low frequency R6G modes are dominated by the charge-transfer terms. The canonical case of adsorbed pyridine is a case where the charge-transfer terms dominate.

In an earlier publication, we analyzed a molecule-like resonance Raman SERS model with a constant coupling strength to one high oscillator strength plasmon state.[12] This model ignores the continuous band structure of Ag. That model did explain the absence of overtones in SERS due to the short resonance-state coherent lifetime, but it did not include the several independent effects in (7). Also note that while the enhanced local field concept is not formally part of this present model, it is included through the self-consistent solution for the coefficients a in (7). That is, the self-consistent electric field appears in the Schrödinger equation that must be solved for the coefficients. In the end this state will give rise to the locally enhanced fields previously discussed in the context of classical electrodynamics. The spatial distribution of the excited-state electron−hole first term in (7) should correspond to the classical $|\mathbf{P(r)}|^2$.

7. Retrospect and Outlook

Confocal microscopic optical techniques, applied to single molecules on single aggregate scattering centers, have led to a new understanding of SERS. It seems likely that in many past ensemble experiments when a relatively low average enhancement was reported, only a few molecules in junctionlike or cracklike sites actually dominated the signal. In addition, the use of Ag colloids with annealed, faceted large Ag particles, rather than the cold deposited rough Ag surfaces of early studies, has led to clearer geometrical models (e.g., Figure 6) for high enhancement sites. Such junction models now allow us to begin rational EM design of Ag particle substrates for practical use of high sensitivity SERS.

The role of electron exchange between molecule and metal points to the importance of Ag and Au as noble metals without surface oxide, in addition to their role as EM field enhancers. In a sense Au is a good SERS substrate for the same reason it is preferred for electrical contacts. In a previous publication we used the analogy of an ac molecular tunneling junction, with SERS corresponding to vibrationally inelastic tunneling. The problem of understanding contacts in single molecule transistors[90] bears some similarity to understanding contacts in SERS; both areas could benefit from fundamental scientific understanding leading to rational contact design.

A clear challenge is bringing the molecule in question into the junction site. In this connection the physics of single molecule optical trapping due to high field gradients should be systematically explored.[91,92] Once in the junction, we need to understand how to minimize photochemistry and blinking dynamics. The excitation spectra of the electronic Raman scattering, molecular Raman scattering, and photochemistry need to be systematically explored, to understand the scattering process and (7), and to optimize practical use. The high enhancement factors of junction SERS are best used at low incident powers to avoid saturation and multiphoton decomposition processes in the junction.

Acknowledgment. This work is supported by the DOE under FG02-98ER14861. We have used MRSEC materials research facilities supported by DMR-0213574. L.B. thanks Mikael Kall, Xiaogang Xu, George Schatz, and Peter Feibelman for suggestions and useful comments.

References and Notes

(1) Moskovits, M. *Rev. Mod. Phys.* **1985**, *57*, 783.
(2) Otto, A.; Mrozek, I.; Grabhorn, H.; Akemann, W. *J. Phys.: Condens. Matter* **1992**, *4*, 1143.
(3) Campion, A.; Kambhampati, P. *Chem. Soc. Rev.* **1998**, *27*, 241.
(4) Nie, S. M.; Emery, S. R. *Science* **1997**, *275*, 1102.
(5) Kneipp, K.; Wang, Y.; Kneipp, H.; Perelman, L. T.; Itzkan, I.; Dasari, R.; Feld, M. S. *Phys. Rev. Lett.* **1997**, *78*, 1667.
(6) Michaels, A. M.; Nirmal, M.; Brus, L. E. *J. Am. Chem. Soc.* **1999**, *121*, 9932.
(7) Xu, H. X.; Bjerneld, E. J.; Kall, M.; Borjesson, L. *Phys. Rev. Lett.* **1999**, *83*, 4357.
(8) Weiss, A.; Haran, G. *J. Phys. Chem. B* **2001**, *105*, 12348.
(9) Kneipp, K.; Kneipp, H.; Itzkan, I.; Dasari, R. R.; Feld, M. S. *Chem. Rev.* **1999**, *99*, 2957.
(10) Moskovits, M.; DiLella, D. P. In *Surface Enhanced Raman Scattering*; Chang, R. K., Furtak, T. E., Eds.; Plenum Press: New York, 1982; p 243.
(11) Lombardi, J. R.; Birke, R. L.; Lu, T.; Xu, J. *J. Chem. Phys.* **1986**, *84*, 4174.

(12) Michaels, A. M.; Jiang, J.; Brus, L. *J. Phys. Chem. B* **2000**, *104*, 11965.
(13) Inoue, M.; Ohtaka, K. *J. Phys. Soc. Jpn.* **1983**, *52*, 3853.
(14) Bosnick, K. A.; Jiang, J.; Brus, L. E. *J. Phys. Chem. B* **2002**, *106*, 8096.
(15) Campion, A.; Ivanecky, J. E.; Child, C. M.; Foster, M. *J. Am. Chem. Soc.* **1995**, *117*, 11807.
(16) Kambhampati, P.; Child, C. M.; Foster, M. C.; Campion, A. *J. Chem. Phys.* **1998**, *108*, 5013.
(17) Jackson, D. *Classical Electrodynamics*, 3rd ed.; John Wiley & Sons: New York, 1999.
(18) Moskovits, M. *J. Chem. Phys.* **1978**, *69*, 4159.
(19) Creighton, J. A.; Blatchford, C. G.; Albrecht, M. G. *J. Chem. Soc., Faraday Trans. 2* **1979**, *75*, 790.
(20) Kerker, M.; Wang, D.-S.; Chew, H. *Appl. Opt.* **1980**, *19*, 4159.
(21) Messinger, B. J.; von Raben, K. U.; Chang, R. K.; Barber, P. W. *Phys. Rev. B* **1981**, *24*, 649.
(22) Kreibig, U.; Vollmer, M. *Optical Properties of Metal Clusters*; Springer-Verlag: New York, 1995.
(23) Klar, T.; Perner, M.; Grosse, S.; von Plessen, G.; Spirkl, W.; Feldmann, J. *Phys. Rev. Lett.* **1998**, *80*, 4249.
(24) Wokaun, A.; Gordon, J. P.; Liao, P. F. *Phys. Rev. Lett.* **1982**, *48*, 957.
(25) Kelly, K. L.; Coronado, E.; Zhao, L. L.; Schatz, G. C. *J. Phys. Chem. B* **2003**, *107*, 668.
(26) Yang, W.-H.; Schatz, G. C.; Van Duyne, R. P. *J. Chem. Phys.* **1995**, *103*, 869.
(27) Kottmann, J. P.; Martin, O. J. F.; Smith, D. R.; Schultz, S. *Phys. Rev. B* **2001**, *64*, 235402.
(28) Liver, N.; Nitzan, A.; Gersten, J. I. *Chem. Phys. Lett.* **1984**, *111*, 449.
(29) Garcia-Vidal, F. J.; Pendry, J. B. *Phys. Rev. Lett.* **1996**, *77*, 1163.
(30) Xu, H. X.; Aizpurua, J.; Kall, M.; Apell, P. *Phys. Rev. E* **2000**, *62*, 4318.
(31) Gersten, J. I. *J. Chem. Phys.* **1980**, *72*, 5779.
(32) Adrian, F. J. *Chem. Phys. Lett.* **1981**, *78*, 45.
(33) Wang, D.-S.; Kerker, M. *Phys. Rev. B* **1981**, *24*, 1777.
(34) Lamprecht, B.; Leitner, A.; Aussenegg, F. R. *Appl. Phys. B* **1997**, *64*, 269.
(35) Crowell, J.; Ritchie, R. H. *Phys. Rev.* **1968**, *172*, 436.
(36) Aravind, P. K.; Nitzan, A.; Metiu, H. *Surf. Sci.* **1981**, *110*, 189.
(37) Kottmann, J. P.; Martin, O. J. F. *Opt. Lett.* **2001**, *26*, 1096.
(38) Kottmann, J. P.; Martin, O. J. F. *Opt. Express* **2001**, *8*, 655.
(39) Xu, M. L.; Dignam, M. J. *J. Chem. Phys.* **1993**, *99*, 2307.
(40) Krug, J. T.; Sánchez, E. J.; Xie, X. S. *J. Chem. Phys.* **2002**, *116*, 10895.
(41) Johnson, P. B.; Christy, R. W. *Phys. Rev. B* **1972**, *6*, 4370.
(42) *Handbook of Optical Constants of Solids*; Palik, E. D., Ed.; Academic Press: Orlando, FL, 1985.
(43) Tian, Z.-Q.; Ren, B.; Wu, D.-Y. *J. Phys. Chem. B* **2002**, *106*, 9463.
(44) Kawabata, A.; Kubo, R. *J. Phys. Soc. Jpn.* **1966**, *21*, 1765.
(45) Veenstra, S. C.; Heeres, A.; Hadziioannou, G.; Sawatzky, G. A.; Jonkman, H. T. *Appl. Phys. A* **2002**, *75*, 661.
(46) Hayashi, N.; Ishii, H.; Ouchi, Y.; Seki, K. *J. Appl. Phys.* **2002**, *92*, 3784.
(47) Wandelt, K. *Appl. Surf. Sci.* **1997**, *111*, 1.
(48) Westcott, S. L.; Averitt, R. D.; Wolfgang, J. A.; Nordlander, P.; Halas, N. J. *J. Phys. Chem. B* **2001**, *105*, 9913.
(49) Nitzan, A.; Brus, L. E. *J. Chem. Phys.* **1981**, *75*, 2205.
(50) Persson, B. N. J. *Chem. Phys. Lett.* **1981**, *82*, 561.
(51) Laufer, G.; Huneke, J. T.; Schaaf, T. F. *Chem. Phys. Lett.* **1981**, *82*, 571.
(52) Mulvaney, P.; Linnert, T.; Henglein, A. *J. Phys. Chem.* **1991**, *95*, 7843.
(53) Henglein, A.; Mulvaney, P.; Linnert, T.; Holzwarth, A. *J. Phys. Chem.* **1992**, *96*, 2411.
(54) Henglein, A. *J. Phys. Chem.* **1993**, *97*, 5457.
(55) Henglein, A. *Chem. Mater.* **1998**, *10*, 444.
(56) Linnert, T.; Mulvaney, P.; Henglein, A. *Ber. Bunsen-Ges. Phys. Chem.* **1991**, *95*, 838.
(57) Gutierrez, M.; Henglein, A. *J. Phys. Chem.* **1993**, *97*, 11368.
(58) Pal, T.; Sau, T. K.; Jana, N. R. *Langmuir* **1997**, *13*, 1481.
(59) Jin, R.; Cao, Y.; Mirkin, C. A.; Kelly, K. L.; Schatz, G. C.; Zheng, J. G. *Science* **2001**, *294*, 1901.
(60) Kamat, P. V. *J. Phys. Chem. B* **2002**, *106*, 7729.
(61) Kapoor, S. *Langmuir* **1998**, *14*, 1021.
(62) Feilchenfeld, H.; Chumanov, G.; Cotton, T. M. *J. Phys. Chem.* **1996**, *100*, 4937.
(63) Mallik, K.; Mandal, M.; Pradhan, N.; Pal, T. *Nano Lett.* **2001**, *1*, 319.
(64) Strelow, F.; Fojtik, A.; Henglein, A. *J. Phys. Chem.* **1994**, *98*, 3032.
(65) Bjerneld, E. J. Ph.D. Thesis, Chalmers University, 2002.
(66) Suh, J. S.; Jang, N. H.; Jeong, D. H.; Moskovits, M. *J. Phys. Chem.* **1996**, *100*, 805.
(67) Jang, N. H.; Suh, J. S.; Moskovits, M. *J. Phys. Chem. B* **1997**, *101*, 8279.
(68) Jeong, D. H.; Suh, J. S.; Moskovits, M. *J. Raman. Spectrosc.* **2001**, *32*, 1026.
(69) Hildebrandt, P.; Stockburger, M. *J. Phys. Chem.* **1984**, *88*, 5935.
(70) Campbell, M.; Lecomte, S.; Smith, W. E. *J. Raman. Spectrosc.* **1999**, *30*, 37.
(71) Birke, R. L.; Lombardi, J. R.; Gersten, J. *Phys. Rev. Lett.* **1979**, *43*, 71.
(72) Otto, A. *Surf. Sci.* **1978**, *75*, L392.
(73) Burstein, E.; Chen, Y. J.; Chen, C. Y.; Lundquist, S.; Tosatti, E. *Solid State Commun.* **1979**, *29*, 567.
(74) Zawadowski, A.; Cardona, M. *Phys. Rev. B* **1990**, *42*, 10732.
(75) Itai, K. *Phys. Rev. B* **1992**, *45*, 707.
(76) Cardona, M. Raman Scattering in High-Tc Superconductors: Phonons, Electrons, and Magnons. In *Raman Scattering in Materials Science*; Weber, W. H., Merlin, R., Eds.; Springer: New York, 2000.
(77) Gass, A. N.; Kapusta, O. I.; Klimin, S. A.; Mal'shukov, A. G. *Solid State Commun.* **1989**, *71*, 749.
(78) Otto, A. *Phys. Status Solidi A: Appl. Res.* **2001**, *188*, 1455.
(79) Portales, H.; Duval, E.; Saviot, L.; Fujii, M.; Sumitomo, M.; Hayashi, S. *Phys. Rev. B* **2001**, *63*, 233402.
(80) Lee, P. C.; Meisel, D. *J. Phys. Chem.* **1982**, *86*, 3391.
(81) Craig, D. P.; Thirunamachandran, T. *Molecular Quantum Electrodynamics*; Dover Publications: New York, 1998.
(82) Levinson, H. J.; Plummer, E. W.; Feibelman, P. J. *Phys. Rev. Lett.* **1979**, *43*, 952.
(83) Feibelman, P. J. *Prog. Surf. Sci.* **1982**, *12*, Section 3A, p 287.
(84) Moskovits, M.; DiLella, D. P.; Maynard, K. J. *Langmuir* **1988**, *4*, 67.
(85) Marini, A.; Del sole, R.; Onida, G. *Phys. Rev. B* **2002**, *66*, 115101.
(86) Nakai, H.; Nakatsuji, H. *J. Chem. Phys.* **1995**, *103*, 2286.
(87) Creighton, J. A. *Surf. Sci.* **1986**, *173*, 655.
(88) Pines, D.; Nozières, P. *The Theory of Quantum Liquids*; Perseus Books: Reading, 1989; Vol. 1.
(89) Yannouleas, C.; Broglia, R. A. *Ann. Phys. (N. Y.)* **1992**, *217*, 105.
(90) Yaliraki, S. N.; Kemp, M.; Ratner, M. A. *J. Am. Chem. Soc.* **1999**, *121*, 3428.
(91) Calander, N.; Willander, M. *Phys. Rev. Lett.* **2002**, *89*, 143603.
(92) Xu, H.; Kall, M. *Phys. Rev. Lett.* **2002**, *89*, 246802.